

STATUS OF TEVATRON RUN II*

V. Lebedev[†]

Fermilab, Batavia, IL 60510, U.S.A.

Abstract

Since the start of Run II, in 2001, the Tevatron collider has demonstrated steady growth of luminosity with a doubling of its integral every 17 months. This paper discusses the present status of the collider, recent improvements that contributed to this impressive luminosity growth, and future plans.

INTRODUCTION

At the beginning of Run II, the luminosity growth was significantly slower than expected. After an analysis of machine operations, beam physics, and engineering issues; a realistic plan for collider improvements was formulated and officially presented at the Department of Energy review in the summer of 2003 [1]. The plan had two scenarios designated the design and base projections. The design projections were based on the success of electron cooling and predicted twice larger integrated luminosity. Since then, the Tevatron luminosity followed the design projections quite closely while some beam parameters have been different. Table I presents parameters of the design projections and typical parameters for 2003 and 2009. Current record collider parameters are: the peak luminosity - $3.47 \cdot 10^{32} \text{ cm}^{-2}\text{s}^{-1}$, and the best weekly luminosity integral - 75 pb^{-1} . Present total Run II luminosity integral is 6.4 fb^{-1} . It is expected that the collider will continue its operations to the end of FY'2011 resulting in total Run II luminosity integral of approximately 12 fb^{-1} (Figure 1.)

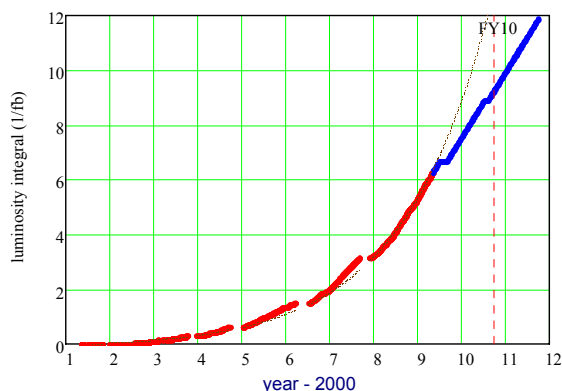


Figure 1: Run II luminosity integral; red – actual, blue – projected, dashed line – an exponential growth with luminosity doubling every 17 months.

The Tevatron operates with two particle detectors CDF

* Work supported by the U.S. Department of Energy under contract No. DE-AC02-76CH03000

[†] val@fnal.gov

¹ 80% availability for antiproton stacking is assumed

and D0. Both detector collaborations have diverse physics programs but the search of the Higgs boson has the highest priority for both of them. Both experiments have analyzed about half of the luminosity integral and have excluded the Higgs boson in the mass region of 160-170 GeV with 95% confidence level [2]. It is expected that by the end of Run II the Higgs boson will be found or excluded if its mass is below 180 GeV - the mass range accessible to Tevatron.

Operation with the peak luminosity of $3.5 \cdot 10^{32} \text{ cm}^{-2}\text{s}^{-1}$ results in ~ 12 inelastic interactions per bunch collision. It was expected in 2003 that the detectors would not be able to operate at such luminosity. However both collaborations demonstrated ability to successfully acquire data at these luminosities and do not see a limit of peak luminosity yet, while both collaborations say it is quite close.

All planned collider upgrades have been implemented and there is not much left for further luminosity growth. Therefore the plan for the rest of the Run II assumes that the collider continues to run with currently achieved luminosity level. However $\sim 10\%$ increase of the weekly luminosity integral before the run ends looks quite possible.

Table I: Planned and Achieved Collider Parameters

| | Apr '03 | Base plan | Apr '09 |
|--|---------|-----------------|---------|
| Average \bar{p} production, 10^{10} /hour | 5.3 | 32 ¹ | 21 |
| Stack to HEP \bar{p} transfer efficiency | 59% | 80% | 80% |
| Protons per bunch, 10^{10} | 20 | 27 | 28 |
| Antiprotons per bunch, 10^{10} | 2.2 | 13 | 8.3 |
| Proton emittance, $\epsilon_{n95\%}$, mm mrad | 20 | 18 | 18 |
| Antiproton emittance, $\epsilon_{n95\%}$, mm mrad | 20 | 18 | 8 |
| Proton bunch length, cm | 62 | 50 | 50 |
| Antiproton bunch length, cm | 58 | 50 | 45 |
| Initial luminosity, $10^{30} \text{ cm}^{-2}\text{s}^{-1}$ | 35 | 290 | 320 |
| Store duration, hour | 20 | 15.2 | 16 |
| Shot setup time, hour | 2 | 2 | 1.5 |
| Store hours per week | 110 | 97 | 110 |
| Weekly luminosity integral, pb^{-1} | 4.7 | 55 | 55 |
| Run II luminosity integral, fb^{-1} | 0.15 | 7.5 | 6.4 |

The driver of luminosity growth during last three years was increase of antiproton production. However the luminosity growth would not be possible if an increase of antiproton production would not be supported by operational improvements in other machines, in particular, in Recycler and Tevatron.

ANTIPROTON STACKING

Antiprotons are produced by the Main Injector (MI) proton beam hitting the antiproton production target every

2.2 s. The antiprotons coming out of the target are focused by the lithium lens to the AP-2 line and transported to the Debuncher where they are stochastically precooled. Then they are transferred to the Accumulator where they are stacked and cooled by stochastic cooling systems.

To achieve desired antiproton flux to the Debuncher the following upgrades have been carried out: (1) Debuncher orbit and optics correction was implemented in 2005 and resulted in acceptance increase from 27 to 35 mm mrad [3], (2) commissioning of slip-stacking in MI [4] together with decrease of Booster longitudinal emittance were finished in 2006 and resulted in the design intensity of $8 \cdot 10^{12}$ protons on the antiproton production target, (3) a new diffusion bonded lithium lens has been brought into operation in 2006 and resulted its gradient increase from 57 to 75 kG/cm, and (4) reduction of stacking cycle period from 2.4 to 2.2 s in 2007. Together with a few other less noticeable improvements it resulted in the antiproton flux coming to Debuncher of $\sim 38 \cdot 10^{10}$ hour⁻¹ ($2.3 \cdot 10^8$ per cycle). This number is sufficiently close to the initial expectation. However the record stacking rate of $\sim 20 \cdot 10^{10}$ hour⁻¹ obtained in February of 2006 was significantly lower. The first rough estimates showed that further improvements of stacking rate are impossible without upgrades of stochastic cooling systems. Detailed computer model of the stacktail system was built at the end of 2006 [5]. Its predictions coincided well with the observed stacking rate. Altogether there are 21 cooling systems in Debuncher and Accumulator. Their upgrades were based on three major blocks: an increase of effective system bandwidth with band equalizers, optics corrections aimed on cooling improvements, and an optimal use or minor modification of existing hardware. Design of amplitude and phase equalizers for each system was based on measurements of the beam response function. The goal of band equalization was to minimize dependence of phase on the frequency and to make the gain linearly growing with frequency [6].

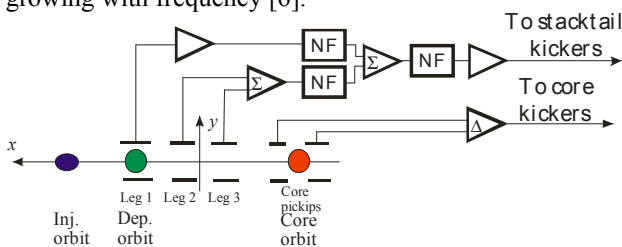


Figure 2: Stacktail system block diagram.

The schematic of stacktail is presented in Figure 2 [7]. The system of pickup electrodes are located in a straight line with large dispersion so that the particles are radially spread in accordance with their energy. The kickers are located in a straight line with zero dispersion. The beam is injected to the injection orbit and then is RF displaced to the deposition orbit where it can be seen by stacktail pickups. The cooling signal is formed as a combination of signals of three pickups. Three notch filters (NF) are tuned to suppress stacktail signal on the beam core. Together with each pickup delay, they also form the

desired dependence of cooling force on the particle momentum. The frequency band of stacktail is 2-4 GHz. Two core cooling systems (2-4 and 4-8 GHz) cool the beam longitudinally in the core.

The van der Meer approximation implies that the cooling system gain, $G(x, \omega)$, depends exponentially on the particle momentum deviation, $x = \Delta p/p$, so that:

$$G(x, \omega) = G(\omega) \exp(x/x_d) \quad (1)$$

Then, the maximum stacktail flux is [5]:

$$J_{\max}(x) = |\eta| W(x)^2 x_d(x) / f_0 \quad (2)$$

where η is the slip factor, and

$$W(x) = \sqrt{\left(\int_0^{\infty} \operatorname{Re}(G(2\pi f)) df \right)^2 / \int_0^{\infty} |G(2\pi f)|^2 \frac{df}{f}} \quad (3)$$

is the effective bandwidth. Note that the same definition of the effective bandwidth is justified for other cooling systems, and in the absence of Schottky band overlap their maximum decrement depends quadratically on the bandwidth.

When the stacktail equalizer was installed in the spring of 2007 the effective bandwidth was increased by 15% from 1.75 to 2 GHz. Additionally in the summer of 2007 we also increased the slip factor in the Accumulator by $\sim 15\%$, and replaced one of the bulk acoustic wave notch filters by a superconducting notch filter having much deeper notches. It suppressed stacktail instabilities at the band edges where the gain was significantly increased by equalizers and insufficient notch filter depth resulted in the instability. However all this work increased the stacking rate to only $\sim 24 \cdot 10^{10}$ hour⁻¹ - still well below expected $30 \cdot 10^{10}$ hour⁻¹. The stacking rate was limited by strong longitudinal and transverse beam heating due to stacktail operation.

Longitudinal core 4-8 GHz equalizer was installed during Summer 2007 shutdown. It increased the system bandwidth by 33% from 3.51 to 4.67 GHz but the improved stacking rate was still below the design value due to the large energy spread coming from the Debuncher.

In contrast to the Accumulator where all stochastic cooling systems operate close to the optimum gain, all Debuncher systems are power limited during most of the cooling cycle. For the Debuncher, the cooling decrement grows as \sqrt{W} and the bandwidth increase yields four times smaller gain than for the optimal gain case. Analysis of possible equalization schemes revealed that only a few percent cooling rate improvement could be achieved. Therefore, we did not pursue this option.

To improve the longitudinal Debuncher cooling we made an upgrade of its notch filter; so that in the first half of the cooling cycle the long leg of the notch filter has one turn delay (as before upgrade) and in the second half of the cycle the delay is switched to two turns. Effectively it doubles the small amplitude cooling rate for the same electronic gain. The two-turn delay notch filter also reduces the momentum acceptance of the cooling system but it is engaged after 1 s of normal cooling, when the beam is already sufficiently cold, and therefore that does

not result in additional particle loss from distribution tails. Figure 3 presents the cooling force for the cases of one and two-turn delay notch filters computed from the measured beam response functions. Computer simulations based on measured cooling system parameters indicated an expected $\sim 10\%$ improvement of the beam momentum spread at the end of cooling cycle. The simulations also showed that the result depends strongly on the notch depth of the filter. Therefore special attention was paid to amplitude balancing of the notch filter legs. Observed cooling improvement was in good agreement with numerical simulations. The final rms momentum spread was $3.2 \cdot 10^{-4}$.

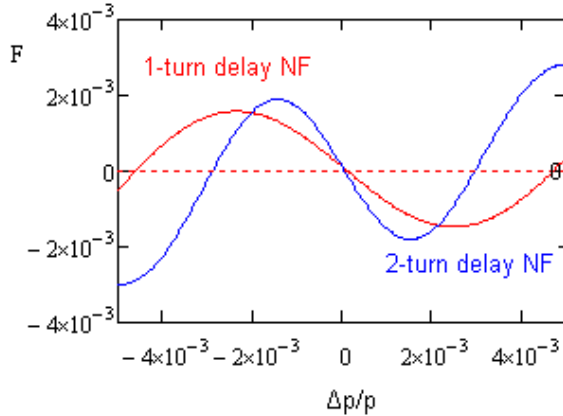


Figure 3: Dependence of cooling force on momentum for 1-turn and 2-turn delay notch filters in Debuncher.

To improve the transverse Debuncher cooling we corrected kicker-to-pickup phase advances, balanced beta-functions in the pickups and kickers of different bands, and introduced two-turn delay notch filters into bands to 3 and 4. The latter decreased common mode and thermal noise contributions to the kicker voltage and allowed a gain increase without increasing power.

All this work resulted in a stacking rate exceeding $30 \cdot 10^{10} \text{ hour}^{-1}$, a good agreement with simulations. Figure 4 presents comparison of measured and observed evolution of the stack during first 100 s of stacking. The vertical lines mark the deposition and core orbits. One can see that there is considerable inverse flux of particles on the left side of deposition orbit (marked by 831). These particles were delivered to the deposition orbit but the stacktail did not pull them into the stack before the next beam pulse. Subsequently, these particles are RF displaced to the left from deposition orbit and lost. It is intensified by small value of cooling force to the left of deposition orbit as shown in Figure 5. Both experiment and numerical model point to the same optimal deposition orbit position where the stacking rate is maximized. Figure 5 shows that this optimal deposition orbit is shifted left from the peak of cooling force. It also explains why the stacking rate is so sensitive to the longitudinal cooling in Debuncher. One can see that the cooling force is reduced by $\sim 30\%$ in the distribution tails for the present width of Debuncher beam. It was worse before Debuncher cooling was improved.

Note also that the peak on the top plot of Figure 4 in vicinity of 800 Hz represents particles left on the injection orbit while major fraction of injected beam is RF displaced to the deposition orbit. If the width of the RF bucket were increased to accept these particles it would increase the number of RF displaced particles backward from the deposition orbit resulting in lower stacking rate.

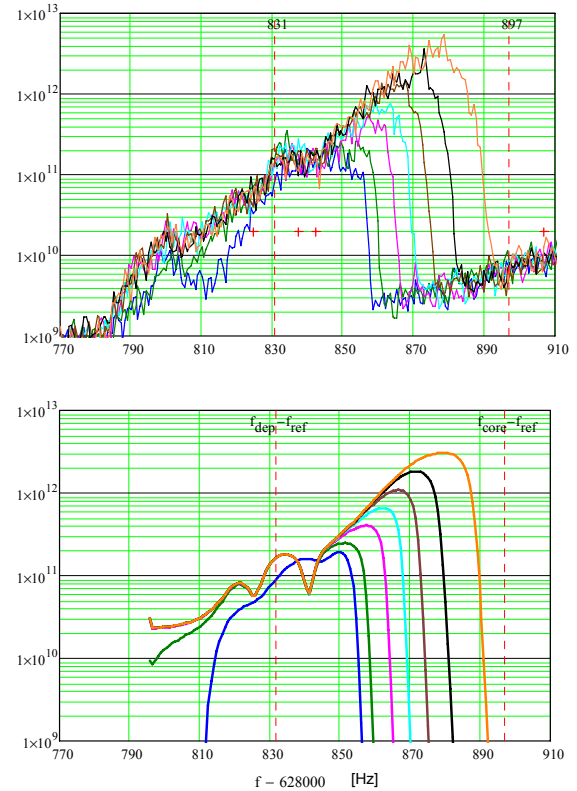


Figure 4: Evolution of particle distribution over revolution frequency during first 100 s of stacking; top - measurements, bottom - simulations. Curves are built at 0.88 s in cycle 1, and 0.22 s in cycles 2,4,7,12,22 and 46.

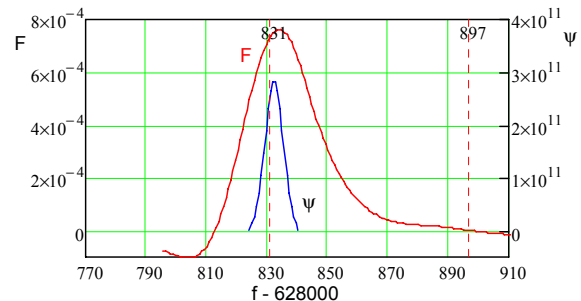


Figure 5: Dependences of cooling force and distribution of particles delivered to the deposition orbit on revolution frequency.

The stacktail gain reconstructed from comparison of simulations and measurements presented in Figure 4 is within $\sim 20\%$ of the optimum gain. Further gain increase is limited by intermodulation distortions in the stacktail TWTs. These amplifiers produce additional noise at core frequencies resulting in the longitudinal core heating.

Two stages of stacktail notch filters suppress the beam Schottky signal by about 60 dB but this suppression is diminished by intermodulation distortions that limit the depth of the notches to ~34 dB at 2.4 GHz and ~26 dB at 3.5 GHz. Correction of these problems requires significant investment and time and is outside the scope of Run II.

Thus improvements of stochastic cooling systems [8] resulted in stacking rate that is ~75% of Debuncher flux; ~5% of the antiprotons are outside of Debuncher cooling range and remain in the Debuncher. The rest are lost in the Accumulator.

The stacking rate is linearly decreased with the stack size. Reduction of the Accumulator-to-Recycler transfer time [9] and cooling improvements in the Recycler allowed us to decrease the maximum stack size and achieve the average stacking rate of $\sim 25 \cdot 10^{10}$ hour⁻¹.

RECYCLER

Since its commissioning in 2005 [10], the Recycler has made a profound effect on the Run II luminosity growth. First, the electron cooling allows cooling of the antiproton beam to significantly higher beam intensity and brightness. Second, availability of an additional antiproton ring allows for small stack sizes in Accumulator. That results in optimal operation of stacktail and maximizes the stacking rate.

Stochastic and electron cooling complement each other. The electron cooling is extremely effective for small amplitudes where cooling time, $\epsilon / (d\epsilon / dt)^{-1}$, is ~7 minutes but is not very effective for particles with large amplitudes. For the particles at the boundary of machine acceptance (40 mm mrad, norm.) the cooling time is longer by about four orders of magnitude – basically resulting no cooling. On the contrary, the stochastic cooling is not very effective for large number of particles but its decrement does not depend on the amplitude and is sufficiently strong to counteract multiple gas scattering, which dramatically improves the beam lifetime.

The intrabeam scattering (IBS) strongly affects the evolution of particle distribution. Recycler operates below the transition energy. Consequently, the 3D beam heating is strongly suppressed. The main source of the heating comes from large variations of beta-functions. They create fast oscillations of the vertical and horizontal “temperatures” resulting in 3D heating. Integration of the heating terms along the ring results in that the temperature exchange between degrees of freedom happens ~6 times faster than the 3D beam heating. For the transverse emittance of 2 mm mrad (95% norm.), the corresponding heating times are 0.2 and 1.2 hours. Because of this, the longitudinal and transverse degrees of freedom are always cooled together. The fast decrease of the electron cooling force with amplitude creates non-Gaussian tails in particle distribution. We use two emittance monitors. The first one is based on flying wires. Its signal is fitted to the Gaussian distribution and, thus, the monitor measures the width of core. The second one is based on the beam Schottky

signals and measures actual rms emittance. Both monitors were calibrated with the proton beam whose distribution is close to Gaussian. However, measurements for the cold antiproton beam are usually different by a factor of ~1.5 due to non-Gaussian tails.

Improvements of cooling have been essential to support the increased Accumulator flux. Stochastic cooling improvements came from installation of equalizers in 2007 and eliminating saturation in medium level electronics of one of the transverse systems. Electron cooling improvements came from a better optics match and a correction of electron beam position in the cooling section [11].

For small beam intensity, the beam lifetime is determined by single gas scattering and is about 700 hours. The lifetime decreases with larger beam intensity. Although the details of particle loss are not known, we presently believe that it is related to the beam space charge. At nominal intensity and emittance ($\sim 350 \cdot 10^{10}$, 2 mm mrad, 95%, norm.) the linear tune shift is ~0.03 and is increased by factor of ~2 during a shot to the Tevatron. To prevent the antiproton beam overcooling and the associated losses the electron beam is shifted from the center of the antiproton beam by 2 mm. This offset is decreased to 0.5 mm during the Tevatron shot.

Large beam space charge not only affects the beam lifetime but also affects the transverse beam stability. It separates coherent and incoherent tunes and suppresses Landau damping [12]. To increase the stability region the bandwidth of the Recycler digital transverse damper was increased to 70 MHz [13]. The higher frequency modes are stabilized by tune spread due to machine chromaticity.

Figure 6 presents typical beam parameters during one cycle of Recycler operation. It starts from a shot to the Tevatron and is finished with the subsequent Tevatron shot.

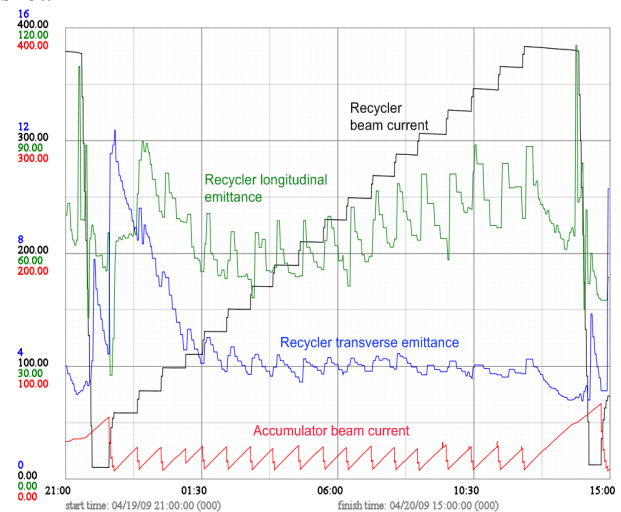


Figure 6: Beam parameters for typical Recycler operation.

TEVATRON

The design projections for the Run II were based on the luminosity evolution model [1]. It takes into account all major diffusion mechanisms (IBS, gas scattering, RF

noise) and particle loss due to diffusion and scattering but ignores the beam-beam effects. Therefore we were comparatively conservative in the choice of beam-beam parameters. Tevatron performance exceeded these expectations. The Tevatron currently operates with large difference between proton and antiproton emittances but both the proton and antiproton beam-beam parameters are sufficiently large, ~ 0.02 , at the store beginning. Figure 7 presents beam intensities for one of the record stores and its comparison with luminosity evolution model. There is a clear demonstration that the intensities of both beams decay faster at the store beginning than the model predictions; and that the proton beam is more subjected to the beam-beam effects. This is happening because protons have ~ 2.5 times larger emittance [14]. Note that the brightness of antiproton beam coming from the Recycler is higher than acceptable and we intentionally increase the antiproton beam emittance from 6 to 8 mm mrad after beam acceleration in Tevatron. While the beam-beam effects have been a serious concern for Tevatron operation their effect on the integrated luminosity is comparatively small – about 10% during most of Run II.

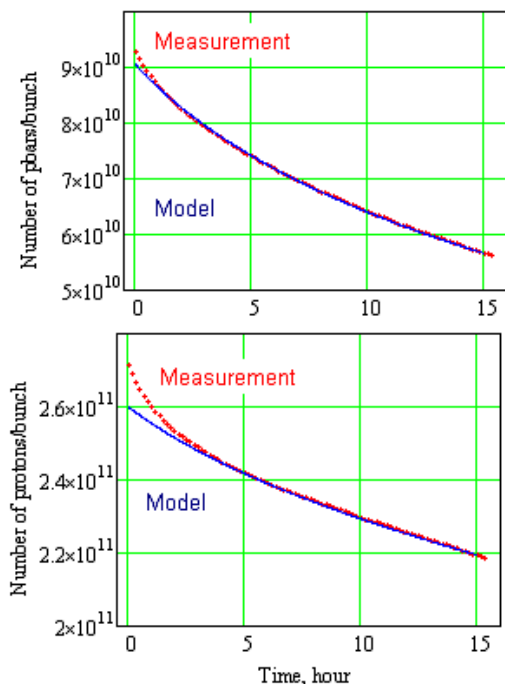


Figure 7: Measured number of particles in proton and antiproton beams on time and its comparison with the luminosity evolution model for store 6950 (Apr. 1, 2009).

The following major improvements were introduced to achieve such performance [15]. The second order chromaticity correction was carried out in 2006. Removing aperture limitation in the vicinity of CDF interaction point occurred in 2007. During the last two years, an improvement of Tevatron stability and operation was a high priority. Better orbit stabilization, persistent current compensation, coupling and chromaticity correction during acceleration, and optimization of transition from injection to collision optics were all part of the effort

Good understanding and correction of linear and non-

linear optics was essential for improvement of Tevatron operation. The Tevatron operates with beta-functions at both interaction points, β^* , equal to about 28 cm. It is lower than the design value of 35 cm. Further reduction of this parameter is limited by aperture and non-linearity of final focus quads and diminishing gain in luminosity due to the hour glass effect. The rms bunch length is changing from ~ 45 cm at the store beginning to ~ 65 cm at its end resulting in the hour glass suppression factor varying from 0.61 to 0.55.

Shortening the shot setup time and other operational improvements [16] has been an important part of the entire effort. Transition from one-bunch acceleration to two-bunch acceleration, as well as improvements in instrumentation and software shortened the average shot setup time from 2 to 1 hour.

Presently about 40% of antiprotons are lost due to nuclear interaction in the interaction points. The luminosity evolution model predicts that if we limit the peak luminosity, the only way to increase the integrated luminosity is an increase of antiproton production and/or a decrease of antiproton loss. An improvement of antiproton coalescing in MI is a most promising way to address it. Potentially it can result in about 10% gain in number of antiprotons delivered to collisions.

The author would like to thank all personnel working on the accelerator part of Run II for their devotion and efforts which made Run II so successful.

REFERENCES

- [1] <http://www-bd.fnal.gov/doereview03/>
- [2] S.P. Griso, *et al.*, “Searches for a high mass Standard Model Higgs boson at the Tevatron,” XLIIIth Rencontres de Moriond QCD and High Energy Interaction, Italy, March 14-21, 2009.
- [3] V. Nagaslaev, *et al.*, EPAC-2006, p. 2050.
- [4] K. Seiya, *et al.*, PAC-2005, p. 347.
- [5] V. Lebedev, COOL-2007, p. 39.
- [6] V. Lebedev, *et al.*, COOL-2007, p. 202.
- [7] R. Pasquinelli, *et al.*, COOL-2007, p.198.
- [8] R. Pasquinelli, *et al.*, “Progress in Antiproton Production at the Fermilab Tevatron Collider,” PAC-2009.
- [9] C. Gattuso, *et al.*, “Improvements to Antiproton Accumulator to Recycler Transfers at the Fermilab Tevatron Collider,” PAC-2009.
- [10] S. Nagaitsev, *et al.*, Phys. Rev. Lett. 96, 044801 (2006).
- [11] Shemyakin, *et al.*, “Optimization of Electron Cooling in the Recycler,” PAC-2009.
- [12] A. Burov, V. Lebedev, Phys. Rev. ST-AB 12, 034201 (2009).
- [13] N. Eddy, *et al.*, EPAC-2008, p. 3254.
- [14] A. Valishev, EPAC 2008, p. 2937.
- [15] Valishev, *et al.*, “Recent Tevatron Operational Experience,” PAC 2009.
- [16] C. Gattuso, *et al.*, Optimization of Integrated Luminosity of the Tevatron,” PAC-2009.